

From Few to More: Scribble-based Medical Image Segmentation via Masked Context Modeling and Continuous Pseudo Labels

Zhisong Wang^{1†}, Yiwen Ye^{1†}, Ziyang Chen¹, Minglei Shu², Yong Xia^{1, 3, 4✉}

¹National Engineering Laboratory for Integrated Aero-Space-Ground-Ocean Big Data Application Technology, School of Computer Science and Engineering, Northwestern Polytechnical University, China

²Shandong Artificial Intelligence Institute, Qilu University of Technology (Shandong Academy of Sciences), China

³Ningbo Institute of Northwestern Polytechnical University, Ningbo 315048, China

⁴Research & Development Institute of Northwestern Polytechnical University in Shenzhen, Shenzhen 518057, China
{zswang, ywye, zychen}@mail.nwpu.edu.cn, shuml@sdas.org, yxia@nwpu.edu.cn

Abstract

Scribble-based weakly supervised segmentation techniques offer comparable performance to fully supervised methods while significantly reducing annotation costs, making them an appealing alternative. Existing methods often rely on auxiliary tasks to enforce semantic consistency and use hard pseudo labels for supervision. However, these methods often overlook the unique requirements of models trained with sparse annotations. Since the model must predict pixel-wise segmentation maps with limited annotations, the ability to handle varying levels of annotation richness is critical. In this paper, we adopt the principle of ‘from few to more’ and propose MaCo, a weakly supervised framework designed for medical image segmentation. MaCo employs masked context modeling (MCM) and continuous pseudo labels (CPL). MCM uses an attention-based masking strategy to disrupt the input image, compelling the model’s predictions to remain consistent with those of the original image. CPL converts scribble annotations into continuous pixel-wise labels by applying an exponential decay function to distance maps, resulting in continuous maps that represent the confidence of each pixel belonging to a specific category, rather than using hard pseudo labels. We evaluate MaCo against other weakly supervised methods using three public datasets. The results indicate that MaCo outperforms competing methods across all datasets, setting a new record in weakly supervised medical image segmentation.

Introduction

Medical image segmentation is essential for preoperative preparation, treatment planning, and prognosis. Recent advancements in deep learning have enabled highly accurate and fast fully automatic segmentation (Panayides et al. 2020; Liu et al. 2021). However, these deep learning methods often require high-quality pixel-wise annotations, which are both time-consuming and labor-intensive. As a promising alternative, weakly supervised semantic segmentation (WSSS) leverages sparse annotations to train models for pixel-wise

predictions. These annotations can include image-level labels, key points, bounding boxes, and scribbles.

Image-level methods typically use a classification branch to generate coarse predictions through class activation maps (CAMs). Key point-based approaches achieve pixel-wise segmentation by identifying either extreme points (Roth et al. 2021; Zhong and Wang 2023) or internal points (En and Guo 2022). Bounding box-based methods generally rely on target similarity analysis within the boxes (Wei et al. 2023) or multi-instance learning (Wang and Xia 2021) to guide model predictions.

While these approaches significantly reduce annotation costs, they often suffer from suboptimal segmentation performance, particularly in complex scenarios, due to the sparse nature of the supervision signals. Scribble-based annotations offer a balanced trade-off between labor costs and segmentation performance. Scribble annotations consist of a few irregular hand-drawn scribbles within target regions. To leverage these scribbles effectively, two main strategies have been proposed: consistency learning (Zhang and Zhuang 2022a,b) and label extension (Liu et al. 2022; Zhou et al. 2023b; Li et al. 2024). Consistency learning methods (Zhang and Zhuang 2022a,b) usually encourage the model to be aware of image semantics. For example, ShapePU (Zhang and Zhuang 2022b) utilized a masked image as an input and forces the model to output a masked prediction. However, learning to predict masked images may not align with the goals of weakly supervised models, which need to learn from sparse annotations and predict pixel-wise labels based on limited information, *i.e.*, from few to more by contextual information. On the other hand, label extension methods typically focus on generating hard pseudo-labels by either utilizing a single branch to select high-quality pseudo-labels through thresholding (Lee and Jeong 2020) or by dynamically mixing predictions from two branches (Luo et al. 2022; Li et al. 2024) to produce a combined prediction. Although these pseudo labels provide richer supervision signals, they can introduce errors, particularly around boundaries, which may mislead the model.

To address these challenges, we propose a weakly supervised framework called **Masked context modeling and Continuous pseudo labels (MaCo)**. MaCo embodies the principle of ‘from few to more’. The masked context model-

[†]Z. Wang and Y. Ye contributed equally to this work. Corresponding author: Y. Xia.

ing (MCM) component encourages the model to infer complete targets from partially corrupted images, while the continuous pseudo labels component enhances the available supervision signals. Specifically, MCM divides an input image into multiple patches and assigns weights to each patch. Instead of using uniform weights (He et al. 2022), we apply attention-based masking using scribbles, assigning higher weights to patches containing scribble pixels. We electively mask patches by initializing them with zeros according to a pre-defined ratio (e.g., 50%). Patches with higher weights have a greater probability of being masked. Finally, we feed both the original and masked images into a UNet for segmentation prediction. The goal is to ensure that the segmentation map from the masked image closely resembles that from the original image, thereby improving the model’s ability to utilize the surrounding context. Furthermore, continuous pseudo labels (CPL) are generated based on the principle that pixels closer to a scribble are more likely to belong to the same category. We calculate distance maps by measuring the Euclidean distance from non-scribble pixels to the nearest scribble pixels and then apply an exponential decay function to transform these distance maps into continuous category-specific labels. These continuous labels provide more nuanced semantic information and confidence levels compared to hard labels, incorporating prior knowledge about the distance from scribbles. Additionally, global category scribbles help refine predictions in the early stages of training. We evaluate MaCo using three public datasets, demonstrating its effectiveness in outperforming existing weakly supervised methods and achieving performance comparable to fully supervised approaches. Furthermore, MaCo maintains robustness under more challenging conditions with fewer training samples or scribble pixels.

Our contributions are three-fold:

- We provide an in-depth analysis of the optimization goals for weakly supervised models based on scribbles, concluding with the principle of ‘from few to more’. Based on this insight, we propose the MaCo framework for weakly supervised medical image segmentation.
- We design masked context modeling and continuous pseudo labels to force the model to enhance the model’s ability to predict semantic information from context and enrich supervision signals, respectively.
- We demonstrate that MaCo outperforms state-of-the-art scribble-based weakly supervised segmentation methods across three public datasets, maintaining performance even with reduced training samples or scribble pixels.

Related Work

Weakly Supervised Medical Segmentation

Medical weakly supervised segmentation aims to train models that can make pixel-wise predictions from sparse annotations, thus reducing annotation costs and attracting significant research interest. Weakly supervised methods use various types of annotations, including image-level, point-level, bounding-box-level, and scribble-level annotations. Image-level annotations provide classification information for each

image. Methods such as those proposed by (Han et al. 2022) and (Zhou et al. 2023c) typically use classification auxiliary paths to generate CAMs for creating coarse pseudo masks. These masks are subsequently refined using multi-layer pseudo-supervision and response thresholds, serving as supervision signals for the segmentation path. Point-level annotations involve either extreme points (Roth et al. 2021; Zhong and Wang 2023) or interior points (En and Guo 2022) for training. For instance, Roth *et al.* (Roth et al. 2021) utilized a random walk algorithm based on extreme points to produce pseudo masks. PSCV (En and Guo 2022) employed interior points and introduces a contrastive variance to enhance model performance by comparing variance distributions across different classes. Bounding-box annotations provide a box around each target. Techniques such as similarity analysis (Wei et al. 2023) and multi-instance learning (Wang and Xia 2021) help models identify targets within these bounding boxes.

Although these annotation types significantly reduce annotation costs, their segmentation performance can be limited, particularly in complex scenarios. Scribble annotations, which consist of a few irregular hand-drawn scribbles per category, offer a promising alternative. Strategies for utilizing scribble annotations fall into two main categories: consistency learning and label extension. Consistency learning (Zhang and Zhuang 2022b; Liu et al. 2022; Zhang and Zhuang 2022a) involves aligning model outputs with those from transformed inputs, which helps the model focus on intrinsic image characteristics and produce more robust results. For example, ShapePU (Zhang and Zhuang 2022b) masks parts of the image and requires the model to predict these masked areas as background, even if targets are present. Similarly, CycleMix (Zhang and Zhuang 2022a) used a mix augmentation strategy and cycle consistency for supervision augmentation. Label extension (Lee and Jeong 2020; Luo et al. 2022; Zhou et al. 2023b; Li et al. 2023, 2024) provides denser information to the model compared to scribbles, mitigating the issue of sparse annotations. S2L (Lee and Jeong 2020) enhanced label extensions for single-branch networks using consistency thresholds. SC-Net (Zhou et al. 2023b) extended scribble annotations into unlabeled regions using a superpixel-guided scribble walking technique, enriching structural information. ScribFormer (Li et al. 2024) integrated a CNN-Transformer structure within encoders to generate pseudo labels by dynamically combining predictions from both CNN and Transformer branches.

Despite these advances, existing scribble-based methods do not fully exploit the potential of weakly supervised models. Our approach, MaCo, builds on the principle of learning more from less information. Unlike consistency learning methods, MaCo disrupts images but predicts undisturbed outcomes. In contrast to label extension methods, MaCo generates continuous pseudo labels rather than hard ones, effectively balancing rich supervision signals with the risk of misleading information.

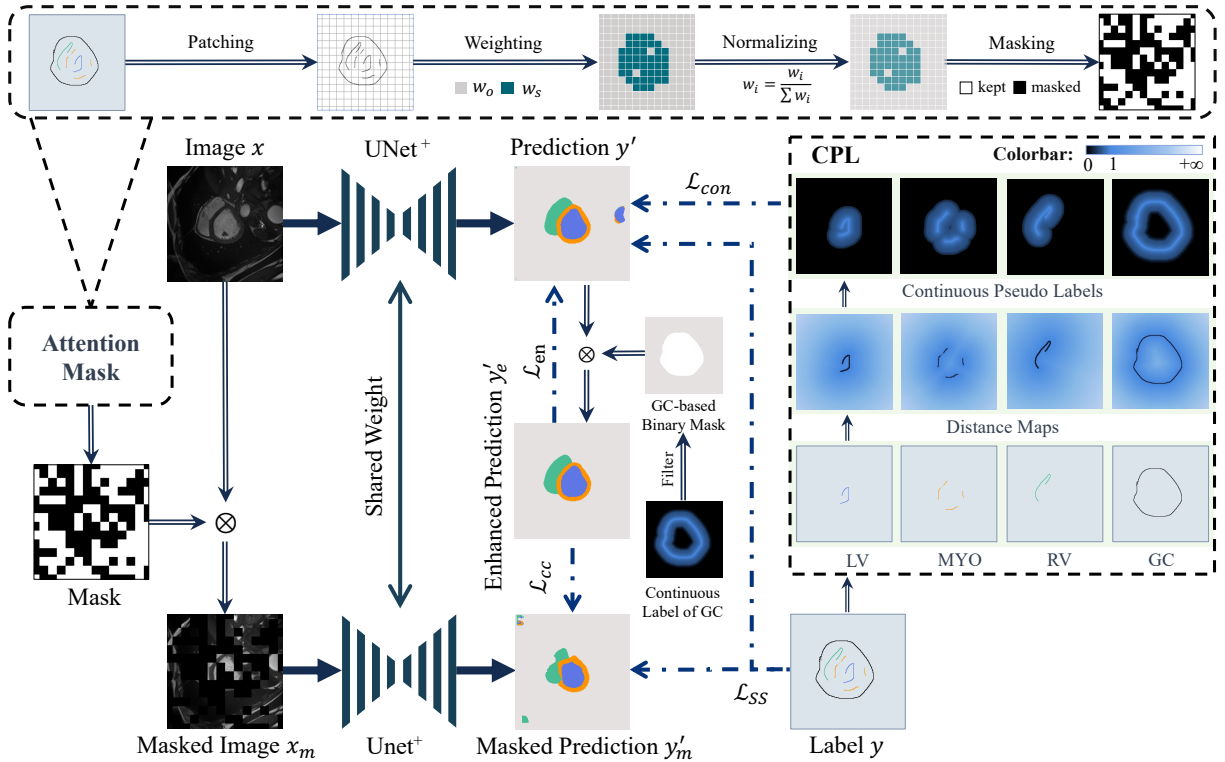


Figure 1: Overview of our MaCo framework. This framework utilizes MCM and CPL. MCM ensures the model produces consistent predictions for both the original image and its masked version. CPL generates continuous pseudo labels that provide rich supervisory signals while minimizing the risk of introducing misleading information.

Masked Image Modeling (MIM)

MIM was initially introduced by MAE (He et al. 2022) as a pretext task for self-supervised learning. This approach involves dividing an image into multiple uniform patches, randomly masking a subset of these patches, and feeding the visible patches to the model. The model is then trained using mean square error loss to predict the masked patches. This technique has shown substantial success in transfer learning (Cai et al. 2022; Jiao et al. 2022; Feng and Zhang 2023; Zhou et al. 2023a; Ye et al. 2024). Subsequently, many studies have applied MIM or its underlying principles to various domains, including image inpainting (Wang et al. 2023), image generation (Chang et al. 2022; Gao et al. 2023), face recognition (Yuan, Zheng, and Dong 2022), multi-view learning (Liu et al. 2024), and action representation learning (Abdelfattah, Hassan, and Alahi 2024). For instance, Imagen Editor (Wang et al. 2023) utilizes an object detector-based masking policy to better handle complex text prompts, resulting in more accurate alignment between generated images and corresponding text. MaskGIT (Chang et al. 2022) employed cosine scheduling as a masking strategy to enhance image generation quality during the decoding phase. MDT (Gao et al. 2023) integrated a masking strategy within the diffusion process to obscure potential image representations during training. In this study, we propose that the capabilities required for the MIM task are closely aligned

with those needed for weakly supervised models. Specifically, predicting patches from highly limited context is analogous to pixel-wise prediction in scribble-based segmentation. Building on this insight, we have developed a masked context modeling approach to integrate this predictive capability into our model.

Methodology

Overview

The proposed MaCo framework is designed around two key components: MCM and CPL. It employs a modified UNet (Baumgartner et al. 2018) as the backbone architecture. During training, both the original image and a masked version, generated through an attention masking operation, are fed into the UNet. The model outputs two predictions, which are trained to achieve maximum similarity. To enhance scribble annotations, we apply an exponential decay function to distance maps, creating category-specific continuous pseudo labels. This approach aims to refine the quality and granularity of the annotations. The overall pipeline of our MaCo is illustrated in Figure 1. We now delve into the details of each part.

MCM Component

To enhance the model’s ability to infer complete targets from partially corrupted images, we introduce MCM as an auxil-

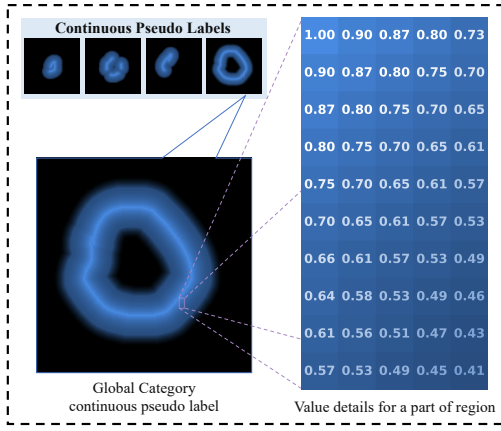


Figure 2: Visualization of the global category continuous pseudo label. The purple boxes indicate the value details within a selected region, showing that the value decreases as the distance from the scribble increases.

ary task. MCM operates as follows. Given an image, we create a masked version based on scribble annotations. The image is partitioned into patches, with each patch assigned a weight depending on whether it contains scribble pixels. Patches with scribble pixels are assigned a weight w_s , and those without receive a lower weight w_o , where $w_s > w_o$. These weights are normalized by dividing each by the sum of all weights, resulting in a probability map. A higher value in this map indicates a higher likelihood of being masked. MCM then masks φ of the patches by setting them to 0, while the remaining patches are set to 1, forming an attention mask. This attention mask is then applied to the original image to produce the masked image. Both the original and masked images are input into a UNet model, producing predictions y' and y'_m , respectively. Moreover, the scribble annotations include both foreground scribbles and global category (GC) scribble. The GC scribble indicates the extent of the target region, ensuring that all targets fall within GC scribble, thus providing an initial estimate of the foreground region. This information is leveraged to refine the prediction y' . Specifically, the pixel with value less than 0.5 are set to 0, while the remaining pixels are set to 1, forming a GC-based binary mask. The enhanced prediction, y'_e , is then obtained by multiplying y' by the GC-based binary mask. To ensure consistency between the predictions, we introduce a context-consistent loss function \mathcal{L}_{cc} , defined as:

$$\mathcal{L}_{cc} = 1 - \frac{y'_m \cdot y'_e}{\|y'_m\| \|y'_e\|}, \quad (1)$$

where $\|\cdot\|$ represents the magnitudes of y'_m and y'_e .

By optimizing \mathcal{L}_{cc} , the model effectively leverages contextual information to infer the semantic content of masked regions, thereby facilitating learning from sparse annotations.

CPL Component

To address the limitations of hard pseudo labels, which can lead to inaccurate predictions and misguide the model, we

propose a method called Continuous Pseudo Labels (CPL) based on distance priors. CPL aims to balance rich supervision signals with potentially misleading information by generating continuous pseudo labels. CPL starts by splitting the scribble annotation into multiple binary annotations, each representing a specific category. For each binary annotation of category c , which includes a set of pixels P^c , the Euclidean distance from each pixel to the nearest scribble pixel is computed. This distance is then converted into a continuous value using an exponential decay function, producing the continuous pseudo label cpl^c , defined as:

$$cpl^c = \{cpl_p^c, p \in P^c\}, \quad (2)$$

$$cpl_p^c = \begin{cases} e^{-0.1 \cdot D(p)} \cdot \mathbb{I}(e^{-0.1 \cdot D(p)} > 0.05), & \text{if } c \neq \text{GC} \\ \max(e^{-0.1 \cdot D(p)}, 0.05), & \text{if } c = \text{GC} \end{cases} \quad (3)$$

where $D(p)$ represents the distance for pixel p , and $\mathbb{I}(\cdot)$ denotes the indicator function. A visualization of cpl^c is provided in Figure 2. In our continuous pseudo labels, pixels closer to the scribble annotation have higher values, ranging from 0 to 1. We set the lower confidence limit to 0.05, as the prior information provided by scribble pixels becomes increasingly unreliable at greater distances. The resultant continuous pseudo labels are then used as supervision signals for y' through the proposed loss function, \mathcal{L}_{con} , formulated as follows:

$$\mathcal{L}_{con} = -\frac{1}{|C||N|} \sum_{c=1}^C p^c \cdot y'_c \log y'_c, \quad (4)$$

where N denotes the number of non-zero elements, and C represents the number of categories.

Scribble-based supervision

Besides, we incorporate a partial Cross-Entropy (pCE) function (Tang et al. 2018), which applies the cross-entropy loss exclusively to the pixels labeled as foreground in the scribble annotations. This is used to compute the scribble supervision loss function, denoted by \mathcal{L}_{ss} , which is defined as:

$$\mathcal{L}_{ss}(y', y'_m) = \mathcal{L}_{pCE}(y') + \lambda_1 \mathcal{L}_{pCE}(y'_m), \quad (5)$$

where λ_1 is a weighting factor.

Similar to \mathcal{L}_{cc} , we also employ $\mathcal{L}_{enhance}$ to align the prediction y' with the enhanced prediction y'_e , thereby improving the model's ability to learn the background category. The enhanced prediction loss \mathcal{L}_{en} is defined as:

$$\mathcal{L}_{en} = 1 - \frac{y' \cdot y'_e}{\|y'\| \|y'_e\|}. \quad (6)$$

The total loss function combines all individual losses and is defined as:

$$\mathcal{L}_{total} = \mathcal{L}_{ss} + \lambda_2 \mathcal{L}_{cc} + \lambda_3 \mathcal{L}_{en} + \lambda_4 \mathcal{L}_{con}, \quad (7)$$

where λ_2 , λ_3 , and λ_4 are weighting factors.

Method	Data	ACDC				MSCMRseg				NCI-ISBI		
		LV	MYO	RV	Avg	LV	MYO	RV	Avg	PZ	CG	Avg
<i>Supervision using scribble annotations</i>												
UNet _{pCE} ⁺	scribbles	79.9	80.1	68.5	76.2	73.4	64.0	49.7	62.4	13.2	26.1	19.7
UNet _{RW} (Grady 2006)	scribbles	85.6	71.4	80.3	79.1	81.9	69.3	76.6	75.9	66.4	74.7	70.6
USTM (Liu et al. 2022)	scribbles	82.4	80.0	82.2	81.5	78.9	67.6	67.6	71.4	52.2	65.4	58.8
DMPLS (Luo et al. 2022)	scribbles	91.7	84.6	86.9	87.7	85.9	76.9	83.7	82.2	30.3	83.4	56.9
SC-Net (Zhou et al. 2023b)	scribbles	89.0	85.1	87.6	87.2	88.3	80.8	86.9	85.3	22.6	80.9	51.8
S2L (Lee and Jeong 2020)	scribbles	80.9	82.3	83.6	82.3	81.7	81.1	72.1	78.3	72.3	63.9	68.1
CycleMix _S (Zhang and Zhuang 2022a)	scribbles	88.3	79.8	86.3	84.8	87.0	73.9	79.1	80.0	66.4	75.7	71.1
ScribFormer (Li et al. 2024)	scribbles	92.2	87.1	87.1	88.8	89.6	81.3	80.7	83.9	63.5	77.4	70.5
nnUNet _{pL} (Gotkowski et al. 2024)	scribbles	84.2	84.3	82.9	83.8	89.5	85.4	87.0	87.3	65.1	83.1	74.1
ShapePU (Zhang and Zhuang 2022b)	scribbles	86.0	79.1	85.2	83.4	91.9	83.2	80.4	85.2	71.6	83.2	77.4
ScribbleVC (Li et al. 2023)	scribbles	91.4	86.6	87.0	88.4	92.1	83.0	85.2	86.8	70.5	81.6	76.1
MaCo	scribbles	93.4	89.2	88.7	90.4	93.1	84.7	87.8	88.5	73.8	87.1	80.5
<i>Supervision using fully-annotated masks</i>												
UNet _F (Ronneberger et al. 2015)	masks	89.2	83.0	78.9	83.7	85.0	72.1	73.8	77.0	72.5	82.2	77.4
CycleMix _F (Zhang and Zhuang 2022a)	masks	91.9	85.8	88.2	88.6	86.4	78.5	78.1	81.0	73.7	84.7	79.2
MaCo _F	masks	94.2	90.9	90.4	91.8	-	-	-	-	77.0	87.8	82.4

Table 1: Results of MaCo, 11 scribble-based methods, and three fully supervised methods across three datasets. The symbol ‘-’ means training masks are unavailable. ‘Avg’ denotes the average result across all foreground categories. The best result in each column is highlighted in **bold**.

\mathcal{L}_{pCE}	\mathcal{L}_{cc}	\mathcal{L}_{mpCE}	\mathcal{L}_{en}	\mathcal{L}_{con}	LV	MYO	RV	Avg
✓					79.9	80.1	68.5	76.2
✓	✓				90.4	88.0	85.6	88.0
✓	✓	✓			92.0	88.1	86.2	88.8
✓	✓	✓	✓		92.3	88.6	87.8	89.6
✓				✓	89.2	85.0	79.4	84.5
✓	✓	✓	✓	✓	93.4	89.2	88.7	90.4

Table 2: Ablation studies of \mathcal{L}_{pCE} , \mathcal{L}_{cc} , \mathcal{L}_{mpCE} , \mathcal{L}_{en} , and \mathcal{L}_{con} on the ACDC dataset. The best result for each column is highlighted in **bold**.

Experiments

Dataset

We evaluated the performance of our MaCo framework using three scribble-based datasets.

ACDC dataset. This dataset (Bernard et al. 2018) consists of cine-MRI scans from 150 patients. Scribble annotations, provided for scans from 100 of these patients (Valvano, Leo, and Tsaftaris 2021), label three categories: left ventricle (LV), right ventricle (RV), and myocardium (MYO). We followed (Li et al. 2024) to partition the dataset into training, validation, and test sets in a 70:15:15 ratio and used training samples corresponding to half of the patients from the training dataset.

MSCMRseg dataset. This dataset (Zhang and Zhuang 2022a) includes late gadolinium enhancement (LGE) MRI scans from 45 patients with cardiomyopathy, annotated for LV, RV, and MYO. Following CycleMix (Zhang and Zhuang

2022a), the dataset is split into 25 scans for training, 5 scans for validation, and 15 scans for testing.

NCI-ISBI dataset. This dataset (Clark et al. 2013) consists of 80 T2-weighted MRI scans from the ISBI 2013 Prostate MRI Challenge. Scribble annotations, provided by (Luo et al. 2022), cover central glands (CG) and peripheral zones (PZ). We randomly divided this dataset into 50 scans for training, 15 scans for validation, and 15 scans for testing.

Implementation Details

We utilized an improved 2D UNet⁺ (Baumgartner et al. 2018) as the backbone for our MaCo framework. All images were resampled to an in-plane resolution of $1.37 \times 1.37 mm^2$ and then cropped to 212×212 using a combination of cropping and padding operations. Each resized image was subsequently normalized to have zero mean and unit variance. Training was conducted over 300 epochs for the ACDC dataset, and 1000 epochs each for the MSCMRseg and NCI-ISBI datasets. We used the Adam optimizer with a learning rate of 0.0001 and a consistent batch size of 4 across all datasets. The weighting factors λ_1 , λ_2 , λ_3 , and λ_4 were empirically set to 0.5, 0.1, 0.1, and 0.1, respectively. All experiments were implemented using Pytorch and trained on one NVIDIA 2080Ti 11GB GPU. The Dice score (Dice) was used as the evaluation metric for all datasets.

Comparing to SOTA Methods

We compared our MaCo with advanced WSSS methods and fully supervised methods on three datasets. The latter is trained on masks with full pixel-wise annotations. The WSSS methods include UNet_{pCE}⁺, UNet_{RW} (Grady 2006),

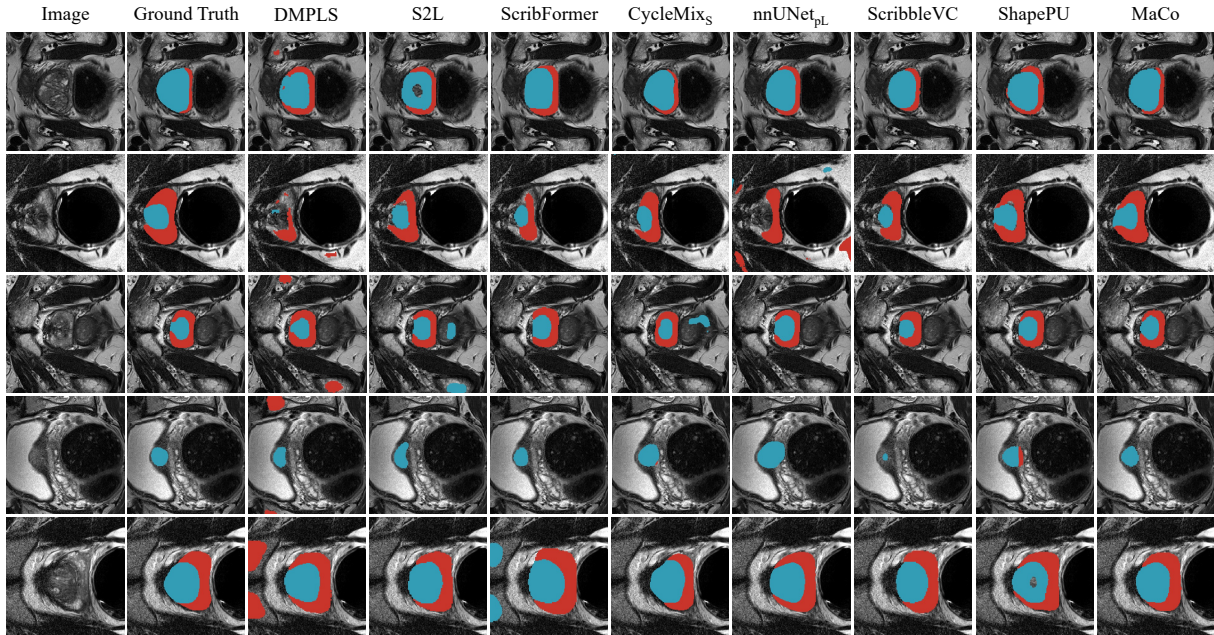


Figure 3: Visualization of segmentation results obtained from seven WSSS methods and MaCo on the NCI-ISBI dataset. Blue and Red are used to color CG and PZ, respectively.

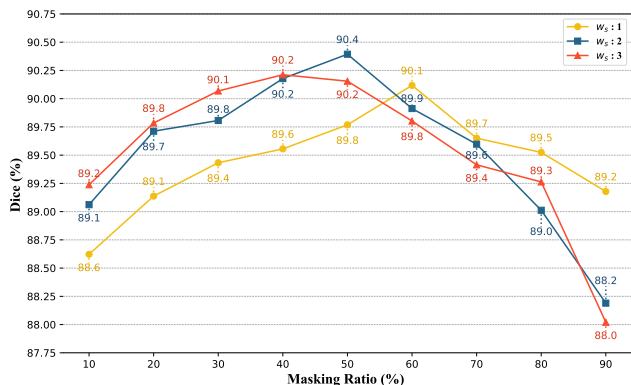


Figure 4: Visualization of the results with different w_s and φ on the ACDC dataset.

USTM (Liu et al. 2022), DMPLS (Luo et al. 2022), SC-Net (Zhou et al. 2023b), S2L (Lee and Jeong 2020), CycleMix_S (Zhang and Zhuang 2022a), ScribFormer (Li et al. 2024), nnUNet_{pL} (Gotkowski et al. 2024), ShapePU (Zhang and Zhuang 2022b), and ScribbleVC (Li et al. 2023). The fully supervised methods include UNet_F (Baumgartner et al. 2018), CycleMix_F (Zhang and Zhuang 2022a), and MaCo_F. We recorded the results of these methods in Table 1. Among them, the results of CycleMix_S (Zhang and Zhuang 2022a), ScribFormer (Li et al. 2024), ShapePU (Zhang and Zhuang 2022b), and ScribbleVC (Li et al. 2023) on the ACDC and MSCMRseg datasets are sourced from their original papers. Moreover, the results of UNet_F (Ronneberger, Fischer, and Brox 2015) and CycleMix_F (Zhang and Zhuang 2022a)

Patch Size	LV	MYO	RV	Avg
4 × 4	92.1	87.8	86.6	88.8
8 × 8	92.6	88.8	88.5	90.0
16 × 16	93.4	89.2	88.7	90.4
24 × 24	92.8	89.1	88.2	90.0
32 × 32	92.7	89.1	87.9	89.9

Table 3: Results of the attention mask strategies with different patch sizes on the ACDC dataset. The best result for each column is highlighted in bold.

on the ACDC and MSCMRseg datasets are from the CycleMix (Zhang and Zhuang 2022a). Compared to scribble-based methods, our MaCo achieves the best performance on most foreground categories across all datasets, except for the MYO segmentation on the MSCMRseg dataset, where our MaCo achieves the second-best performance. The significant improvement of 1.6%, 1.2%, and 3.1% on three datasets demonstrate the superior performance of our MaCo. Compared to fully supervised methods, our MaCo achieves better performance across all datasets than UNet_F (Ronneberger, Fischer, and Brox 2015) and CycleMix_F (Zhang and Zhuang 2022a) and small performance gaps over our baseline MaCo_F, while significantly reducing the annotation costs.

Ablation Studies

We evaluated the effectiveness of four proposed loss functions, including \mathcal{L}_{cc} , \mathcal{L}_{mpCE} , \mathcal{L}_{en} , and \mathcal{L}_{con} , and the results are presented in Table 2. The first row of the table rep-

Data Sensitivity	LV	MYO	RV	Avg
Shrink Ratio				
0	93.4	89.2	88.7	90.4
10	93.1	89.2	87.8	90.0
20	92.1	88.6	86.8	89.2
30	92.3	88.8	85.2	88.8
40	92.0	88.3	84.3	88.2
50	91.5	87.9	82.7	87.4
Training Sample Number				
14	90.1	85.7	82.4	86.1
28	90.8	87.1	87.2	88.4
35	93.4	89.2	88.7	90.4
56	93.3	89.6	88.9	90.6
70	93.5	89.5	90.7	91.2

Table 4: Results of MaCo with different shrink ratios and training sample numbers on the ACDC dataset. The shrink ratio means the ratio of masked pixels for each category on an image.

resents the baseline model, which was trained exclusively using the available scribble annotations. Our findings lead to the following conclusions. First, the baseline with \mathcal{L}_{cc} , which corresponds to the proposed MCM, significantly outperforms the baseline across all segmentation metrics, showing improvements of 10.5%, 7.9%, and 17.1% in LV, MYO, and RV, respectively. Second, incorporating \mathcal{L}_{mpCE} and \mathcal{L}_{en} yields further performance gains, resulting in an additional improvement of 1.6% in the averaged Dice score. Third, the baseline with \mathcal{L}_{con} , corresponding to the proposed CPL, also surpasses the baseline performance across all metrics, providing an 8.3% average gain in Dice scores. Fourth, when combining all four loss functions, the proposed MaCo achieves the highest Dice scores across LV, MYO, and RV, demonstrating the overall effectiveness of these loss functions in improving the performance of weakly supervised segmentation models.

Visualization of Segmentation Results

For qualitative analysis, we selected five images from the NCI-ISBI dataset and compared the segmentation results from seven WSSS methods and our MaCo, with the images and ground truths, as shown in Figure 3. These visualizations reveal that the segmentation outputs from MaCo most closely match the ground truths compared to the other WSSS methods. For example, in the last row, MaCo’s results exhibit the best alignment in shape and size with the ground truth, effectively addressing issues such as target omission and overfitting that are evident in the other methods.

Parameter Settings

In the proposed MaCo framework, three key hyperparameters significantly influence segmentation performance: the weight w_s for patches containing scribble pixels, the masking ratio φ , and the patch size used in

MCM. We assessed the impact of these hyperparameters through experiments on the ACDC dataset. First, we explored the effects of w_s and φ . The values of w_s were tested at $\{1, 2, 3\}$, and φ was varied across 10%, 20%, 30%, 40%, 50%, 60%, 70%, 80%, 90%. The results, shown in Figure 4, prove that increasing φ initially leads to a sharp improvement in segmentation performance, which later declines significantly. Furthermore, higher values of w_s exhibit better performance at lower masking ratios but worsen at higher ratios. The optimal settings were found to be $w_s = 2$ and $\varphi = 50\%$. Next, we investigated the effect of patch size by testing various dimensions: 4×4 , 8×8 , 16×16 , 24×24 , and 32×32 . For dimensions that did not evenly divide the image, zero-padding was applied before patch division. The results, summarized in Table 3, indicate that a patch size of 16×16 provides the best performance.

Based on these findings, the settings adopted for our experiments were $w_s = 2$, $\varphi = 50\%$, and a patch size of 16×16 .

Data Sensitivity Study

We investigated the sensitivity of our MaCo framework to the richness of supervision signals by varying shrink ratios and training sample sizes on the ACDC dataset. Two strategies were employed to reduce supervision signals: reducing the number of scribbles per image (as detailed in the Appendix) and decreasing the total number of samples. The results are shown in Table 4. It reveals that as the proportion of masked scribble pixels increases, the performance of MaCo gradually declines. Despite masking 50% of the scribble pixels, MaCo retains approximately 96.7% of its performance compared to using the full set of scribbles. This indicates that MaCo performs well even with sparse annotations, demonstrating its robustness to variations in supervision signal richness. Moreover, as the number of training samples increased from 14 to 70, the performance of MaCo improved from 86.1% to 91.2% in terms of the averaged Dice score. It suggests that MaCo’s segmentation performance can be further enhanced with the availability of additional scribble annotations.

Conclusion

In this paper, we propose MaCo, a weakly supervised framework that leverages MCM and CPL for medical image segmentation. Adopting the principle of ‘from few to more’, MCM encourages the model to align predictions from both the original and masked versions of an image, thereby improving its capacity to infer semantic information from contextual clues. CPL provides continuous pseudo labels, balancing rich supervisory signals with potentially ambiguous information. Our experiments on three scribble-based segmentation datasets demonstrated the effectiveness of the proposed MaCo. In the future, we will continue to investigate methods to enhance the model’s ability of ‘from few to more’.

Acknowledgments

This work was supported in part by the National Natural Science Foundation of China under Grants 62171377, in part by the Ningbo Clinical Research Center for Medical Imaging under Grant 2021L003 (Open Project 2022LYKFZD06), and in part by Shenzhen Science and Technology Program under Grants JCYJ20220530161616036.

Appendix

More training samples on the ACDC dataset

In the section titled ‘Comparing to SOTA Methods’, we compared our MaCo approach with other advanced WSSS methods using 35 training samples from the ACDC dataset, aligning with the most commonly used benchmark. To further assess the effectiveness of MaCo, we conducted additional experiments using a larger set of training samples (70 samples, encompassing the entire training set of the ACDC dataset). The competing methods include UNet_{RW} (Grady 2006), ShapePU (Zhang and Zhuang 2022b), USTM (Liu et al. 2022), nnUNet (Gotkowski et al. 2024), S2L (Lee and Jeong 2020), CycleMix_S (Zhang and Zhuang 2022a), DMPLS (Luo et al. 2022), ScribbleVC (Li et al. 2023), SC-Net (Zhou et al. 2023b), and ScribFormer (Li et al. 2024). The results were shown in Table 5. Note that the results for CycleMix_S (Zhang and Zhuang 2022a) and ScribFormer (Li et al. 2024) were sourced from their respective original papers. Our observations reveal that MaCo consistently outperforms all competing methods across all evaluated categories. Specifically, MaCo improves Dice scores by 0.9% for LV, 1.8% for MYO, 2.8% for RV, and 1.8% on average. These results further demonstrate the superior performance of MaCo.

Method	LV	MYO	RV	Avg
UNet _{RW}	87.2	71.6	80.8	79.9
ShapePU	86.0	81.3	85.4	84.2
USTM	86.3	79.8	84.0	83.4
nnUNet _{pL}	88.8	82.0	84.6	85.1
S2L	85.6	84.2	85.8	85.2
CycleMix _S	88.0	82.5	86.0	85.5
DMPLS	92.0	86.1	86.6	88.2
ScribbleVC	92.1	87.1	87.5	88.9
SC-Net	91.9	87.5	87.9	89.1
ScribFormer	92.6	87.7	87.8	89.4
MaCo	93.5	89.5	90.7	91.2

Table 5: Results of MaCo and 10 competing WSSS methods on the ACDC dataset with 70 training samples. The best result for each column is highlighted in **bold**.

Ablation studies on MSCMRseg and NCI-ISBI datasets

We conducted ablation studies on the MSCMRseg and NCI-ISBI datasets to evaluate the effectiveness of the proposed loss functions \mathcal{L}_{cc} , \mathcal{L}_{mpCE} , \mathcal{L}_{en} , and \mathcal{L}_{con} , as shown in Table 6 and 7. First, the baseline model with \mathcal{L}_{cc} , corresponding

\mathcal{L}_{pCE}	\mathcal{L}_{cc}	\mathcal{L}_{mpCE}	\mathcal{L}_{en}	\mathcal{L}_{con}	LV	MYO	RV	Avg
✓					73.4	64.0	49.7	62.4
✓	✓				88.6	73.7	79.3	80.5
✓	✓	✓			91.3	82.6	86.8	86.9
✓	✓	✓	✓		92.2	83.9	86.7	87.6
✓				✓	82.8	74.4	73.6	76.9
✓	✓	✓	✓	✓	93.1	84.7	87.8	88.5

Table 6: Ablation studies of \mathcal{L}_{pCE} , \mathcal{L}_{cc} , \mathcal{L}_{mpCE} , \mathcal{L}_{en} , and \mathcal{L}_{con} on the MSCMRseg dataset. The best result for each column is highlighted in **bold**.

\mathcal{L}_{pCE}	\mathcal{L}_{cc}	\mathcal{L}_{mpCE}	\mathcal{L}_{en}	\mathcal{L}_{con}	PZ	CG	Avg
✓					13.2	26.1	19.7
✓	✓				52.0	66.3	59.2
✓	✓	✓			64.4	73.3	68.9
✓	✓	✓	✓		66.2	83.1	74.7
✓				✓	28.2	57.7	43.0
✓	✓	✓	✓	✓	73.8	87.1	80.5

Table 7: Ablation studies of \mathcal{L}_{pCE} , \mathcal{L}_{cc} , \mathcal{L}_{mpCE} , \mathcal{L}_{en} , and \mathcal{L}_{con} on the NCI-ISBI dataset. The best result for each column is highlighted in **bold**.

to the proposed MCM, significantly outperformed the baseline across all segmentation metrics. Notably, the average Dice scores on the MSCMRseg and NCI-ISBI datasets increased by 18.1% and 39.5%, respectively. Second, incorporating \mathcal{L}_{mpCE} and \mathcal{L}_{en} yields further performance gains, resulting in an additional improvement of 7.1% and 15.5% in the average Dice score across both datasets. Third, the baseline with \mathcal{L}_{con} , corresponding to the proposed CPL, also surpasses the baseline performance across all metrics, providing a 14.5% and 23.3% average gain in Dice scores. Fourth, when combining all four loss functions, the proposed MaCo achieves the highest Dice scores on both the MSCMRseg and NCI-ISBI datasets, demonstrating the overall effectiveness of these loss functions in enhancing the performance of weakly supervised segmentation models.

Scribble shrink ratio

In the ‘Data Sensitivity Study’ section, we reduced the number of scribble pixels per image to evaluate the robustness and data sensitivity of the proposed MaCo method. In this section, we provided a detailed explanation of how the scribble shrink ratio is achieved. Specifically, for a given shrink ratio, we first calculated the number of pixels to be masked. We then identified all connected regions within the scribbles and processed them sequentially. When processing a connected region, if masking all pixels in that region does not exceed the required number, we proceed to mask the entire region. If masking the entire region would exceed the required number, we selectively mask a portion of the pixels to meet the required count while ensuring that the remaining pixels within the region remain contiguous. We visualized the resulting masked scribble labels with shrink ratios

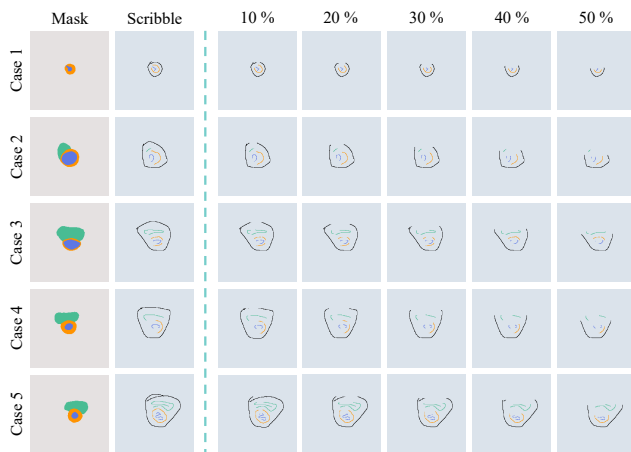


Figure 5: Visualization of scribble annotations for five samples with shrink ratios of 10%, 20%, 30%, 40%, and 50%.

Decay Factor	LV	MYO	RV	Avg
0.05	92.7	88.9	88.8	90.1
0.1	93.4	89.2	88.7	90.4
0.2	92.5	89.0	88.4	90.0
0.5	92.0	88.6	88.5	89.7

Table 8: Results of different delay factors on the ACDC Dataset.

of 10%, 20%, 30%, 40%, and 50%, as illustrated in Figure 5. Unlike random masking of scribble pixels, our approach sequentially masks scribbles to better simulate the actual annotation process, where an annotator incrementally increases the number of scribbles, rather than simply increasing the number of scribble pixels.

Impact of different decay factors

In Equation 3, we employed an exponential decay function to transform the distance map into a continuous map. Specifically, we used the exponential decay function $e^{-0.1 \cdot D(p)}$, setting the decay factor to 0.1. In this section, we explore the effects of varying the decay factor by experimenting with values of 0.05, 0.2, and 0.5. The results of these experiments are presented in Table 8. Our findings indicate that a decay factor of 0.1 yields the best generalization performance. Additionally, we visualized the continuous pseudo-labels for each category with decay factors of 0.05, 0.1, 0.2, and 0.5, as shown in Figure 6. We observed that smaller decay factors produce continuous pseudo-labels with broader confidence regions, offering richer information but also introducing more noise compared to larger decay factors. Ultimately, setting the decay factor to 0.1 strikes an effective balance between informative richness and noise reduction.

References

Abdelfattah, M.; Hassan, M.; and Alahi, A. 2024. MaskCLR: Attention-Guided Contrastive Learning for Ro-

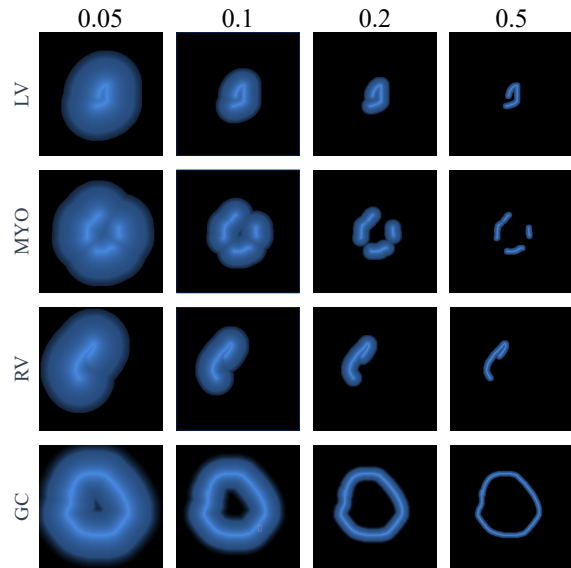


Figure 6: Visualization of the continuous pseudo labels of LV, MYO, RV, and GC on the ACDC dataset with delay factors of 0.05, 0.1, 0.2, and 0.5, respectively.

bust Action Representation Learning. In *Proceedings of the IEEE/CVF Conference on Computer Vision and Pattern Recognition*, 18678–18687.

Baumgartner, C. F.; Koch, L. M.; Pollefeys, M.; and Konukoglu, E. 2018. An exploration of 2D and 3D deep learning techniques for cardiac MR image segmentation. In *Statistical Atlases and Computational Models of the Heart. ACDC and MMWHS Challenges: 8th International Workshop, STACOM 2017, Held in Conjunction with MICCAI 2017, Quebec City, Canada, September 10-14, 2017, Revised Selected Papers 8*, 111–119. Springer.

Bernard, O.; Lalonde, A.; Zotti, C.; Cervenansky, F.; Yang, X.; Heng, P.-A.; Cetin, I.; Lekadir, K.; Camara, O.; Ballester, M. A. G.; et al. 2018. Deep learning techniques for automatic MRI cardiac multi-structures segmentation and diagnosis: is the problem solved? *IEEE transactions on medical imaging*, 37(11): 2514–2525.

Cai, Z.; Lin, L.; He, H.; and Tang, X. 2022. Uni4Eye: unified 2D and 3D self-supervised pre-training via masked image modeling transformer for ophthalmic image classification. In *International Conference on Medical Image Computing and Computer-Assisted Intervention*, 88–98. Springer.

Chang, H.; Zhang, H.; Jiang, L.; Liu, C.; and Freeman, W. T. 2022. Maskgit: Masked generative image transformer. In *Proceedings of the IEEE/CVF Conference on Computer Vision and Pattern Recognition*, 11315–11325.

Clark, K.; Vendt, B.; Smith, K.; Freymann, J.; Kirby, J.; Koppel, P.; Moore, S.; Phillips, S.; Maffitt, D.; Pringle, M.; et al. 2013. The Cancer Imaging Archive (TCIA): maintaining and operating a public information repository. *Journal of digital imaging*, 26: 1045–1057.

En, Q.; and Guo, Y. 2022. Annotation by clicks: A point-

- supervised contrastive variance method for medical semantic segmentation. *arXiv preprint arXiv:2212.08774*.
- Feng, Z.; and Zhang, S. 2023. Evolved part masking for self-supervised learning. In *Proceedings of the IEEE/CVF Conference on Computer Vision and Pattern Recognition*, 10386–10395.
- Gao, S.; Zhou, P.; Cheng, M.-M.; and Yan, S. 2023. Masked diffusion transformer is a strong image synthesizer. In *Proceedings of the IEEE/CVF International Conference on Computer Vision*, 23164–23173.
- Gotkowsky, K.; Lüth, C.; Jäger, P. F.; Ziegler, S.; Krämer, L.; Denner, S.; Xiao, S.; Disch, N.; Maier-Hein, K. H.; and Isensee, F. 2024. Embarrassingly Simple Scribble Supervision for 3D Medical Segmentation. *arXiv preprint arXiv:2403.12834*.
- Grady, L. 2006. Random walks for image segmentation. *IEEE transactions on pattern analysis and machine intelligence*, 28(11): 1768–1783.
- Han, C.; Lin, J.; Mai, J.; Wang, Y.; Zhang, Q.; Zhao, B.; Chen, X.; Pan, X.; Shi, Z.; Xu, Z.; et al. 2022. Multi-layer pseudo-supervision for histopathology tissue semantic segmentation using patch-level classification labels. *Medical Image Analysis*, 80: 102487.
- He, K.; Chen, X.; Xie, S.; Li, Y.; Dollár, P.; and Girshick, R. 2022. Masked autoencoders are scalable vision learners. In *Proceedings of the IEEE/CVF conference on computer vision and pattern recognition*, 16000–16009.
- Jiao, M.; Liu, H.; Yang, Z.; Tian, S.; Ouyang, H.; Li, Y.; Yuan, Y.; Liu, J.; Wang, C.; Lang, N.; et al. 2022. Self-supervised Learning Based on a Pre-trained Method for the Subtype Classification of Spinal Tumors. In *International Workshop on Computational Mathematics Modeling in Cancer Analysis*, 58–67. Springer.
- Lee, H.; and Jeong, W.-K. 2020. Scribble2label: Scribble-supervised cell segmentation via self-generating pseudo-labels with consistency. In *Medical Image Computing and Computer Assisted Intervention—MICCAI 2020: 23rd International Conference, Lima, Peru, October 4–8, 2020, Proceedings, Part I 23*, 14–23. Springer.
- Li, Z.; Zheng, Y.; Luo, X.; Shan, D.; and Hong, Q. 2023. Scribblevc: Scribble-supervised medical image segmentation with vision-class embedding. In *Proceedings of the 31st ACM International Conference on Multimedia*, 3384–3393.
- Li, Z.; Zheng, Y.; Shan, D.; Yang, S.; Li, Q.; Wang, B.; Zhang, Y.; Hong, Q.; and Shen, D. 2024. ScribFormer: Transformer Makes CNN Work Better for Scribble-based Medical Image Segmentation. *IEEE Transactions on Medical Imaging*.
- Liu, C.; Wen, J.; Liu, Y.; Huang, C.; Wu, Z.; Luo, X.; and Xu, Y. 2024. Masked two-channel decoupling framework for incomplete multi-view weak multi-label learning. *Advances in Neural Information Processing Systems*, 36.
- Liu, X.; Song, L.; Liu, S.; and Zhang, Y. 2021. A review of deep-learning-based medical image segmentation methods. *Sustainability*, 13(3): 1224.
- Liu, X.; Yuan, Q.; Gao, Y.; He, K.; Wang, S.; Tang, X.; Tang, J.; and Shen, D. 2022. Weakly supervised segmentation of COVID19 infection with scribble annotation on CT images. *Pattern recognition*, 122: 108341.
- Luo, X.; Hu, M.; Liao, W.; Zhai, S.; Song, T.; Wang, G.; and Zhang, S. 2022. Scribble-supervised medical image segmentation via dual-branch network and dynamically mixed pseudo labels supervision. In *International Conference on Medical Image Computing and Computer-Assisted Intervention*, 528–538. Springer.
- Panayides, A. S.; Amini, A.; Filipovic, N. D.; Sharma, A.; Tsaftaris, S. A.; Young, A.; Foran, D.; Do, N.; Golemati, S.; Kurc, T.; et al. 2020. AI in medical imaging informatics: current challenges and future directions. *IEEE journal of biomedical and health informatics*, 24(7): 1837–1857.
- Ronneberger, O.; Fischer, P.; and Brox, T. 2015. U-net: Convolutional networks for biomedical image segmentation. In *Medical image computing and computer-assisted intervention—MICCAI 2015: 18th international conference, Munich, Germany, October 5-9, 2015, proceedings, part III 18*, 234–241. Springer.
- Roth, H. R.; Yang, D.; Xu, Z.; Wang, X.; and Xu, D. 2021. Going to extremes: weakly supervised medical image segmentation. *Machine Learning and Knowledge Extraction*, 3(2): 507–524.
- Tang, M.; Djelouah, A.; Perazzi, F.; Boykov, Y.; and Schroers, C. 2018. Normalized cut loss for weakly-supervised cnn segmentation. In *Proceedings of the IEEE conference on computer vision and pattern recognition*, 1818–1827.
- Valvano, G.; Leo, A.; and Tsaftaris, S. A. 2021. Learning to segment from scribbles using multi-scale adversarial attention gates. *IEEE Transactions on Medical Imaging*, 40(8): 1990–2001.
- Wang, J.; and Xia, B. 2021. Bounding box tightness prior for weakly supervised image segmentation. In *International conference on medical image computing and computer-assisted intervention*, 526–536. Springer.
- Wang, S.; Saharia, C.; Montgomery, C.; Pont-Tuset, J.; Noy, S.; Pellegrini, S.; Onoe, Y.; Laszlo, S.; Fleet, D. J.; Soricut, R.; et al. 2023. Imagen editor and editbench: Advancing and evaluating text-guided image inpainting. In *Proceedings of the IEEE/CVF conference on computer vision and pattern recognition*, 18359–18369.
- Wei, J.; Hu, Y.; Cui, S.; Zhou, S. K.; and Li, Z. 2023. Weakpolyp: You only look bounding box for polyp segmentation. In *International Conference on Medical Image Computing and Computer-Assisted Intervention*, 757–766. Springer.
- Ye, Y.; Xie, Y.; Zhang, J.; Chen, Z.; Wu, Q.; and Xia, Y. 2024. Continual self-supervised learning: Towards universal multi-modal medical data representation learning. In *Proceedings of the IEEE/CVF Conference on Computer Vision and Pattern Recognition*, 11114–11124.
- Yuan, G.; Zheng, H.; and Dong, J. 2022. Msml: Enhancing occlusion-robustness by multi-scale segmentation-based

mask learning for face recognition. In *Proceedings of the AAAI Conference on Artificial Intelligence*, 3197–3205.

Zhang, K.; and Zhuang, X. 2022a. Cyclemix: A holistic strategy for medical image segmentation from scribble supervision. In *Proceedings of the IEEE/CVF Conference on Computer Vision and Pattern Recognition*, 11656–11665.

Zhang, K.; and Zhuang, X. 2022b. Shapepu: A new pu learning framework regularized by global consistency for scribble supervised cardiac segmentation. In *International Conference on Medical Image Computing and Computer-Assisted Intervention*, 162–172. Springer.

Zhong, Y.; and Wang, Y. 2023. SimPLe: Similarity-aware propagation learning for weakly-supervised breast cancer segmentation in DCE-MRI. In *International Conference on Medical Image Computing and Computer-Assisted Intervention*, 567–577. Springer.

Zhou, L.; Liu, H.; Bae, J.; He, J.; Samaras, D.; and Prasanna, P. 2023a. Self pre-training with masked autoencoders for medical image classification and segmentation. In *2023 IEEE 20th International Symposium on Biomedical Imaging (ISBI)*, 1–6. IEEE.

Zhou, M.; Xu, Z.; Zhou, K.; and Tong, R. K.-y. 2023b. Weakly supervised medical image segmentation via superpixel-guided scribble walking and class-wise contrastive regularization. In *International Conference on Medical Image Computing and Computer-Assisted Intervention*, 137–147. Springer.

Zhou, Y.; Wu, Y.; Wang, Z.; Wei, B.; Lai, M.; Shou, J.; Fan, Y.; and Xu, Y. 2023c. Cyclic learning: Bridging image-level labels and nuclei instance segmentation. *IEEE Transactions on Medical Imaging*.